Supplement of Atmos. Chem. Phys., 21, 3491–3506, 2021
https://doi.org/10.5194/acp-21-3491-2021-supplement

Atmospheric Chemistry and Physics
Open Access
EGU

Supplement of

Size-resolved atmospheric ice-nucleating particles during East Asian dust events

Jingchuan Chen et al.

Correspondence to: Zhijun Wu (zhijunwu@pku.edu.cn)

1. Supplementary Tables

Table S1. The criteria used to distinguish between dust and non-dust events for 14 sets of samples.

The two weather conditions, i.e., dust and non-dust events, were defined based on PM_{10} mass concentration (PM_{10} Mass Conc.), the volume concentration of coarse mode particles (Vol. Conc.), phenomenological dust storm observations operated by China Meteorological Administration (Observations by CMA), and the concentration of aluminium (Al).

Sample ID	PM_{10} Mass Conc.[1]	Vol. Conc.[2]	Observations by CMA [3]	Concentration of Al element (μg m^{-3}) [4]	Weather condition
M1	True	True	True	5.65	Dust
M2	True	True	True	1.68	Dust
M3	True	True	True	0.72	Dust
M4	True	False	False	0.04	Non-dust [5]
M5	True	False	True	0.12	Dust
M6	True	True	True	1.45	Dust
M7	True	True	True	1.07	Dust
M8	True	True	True	1.01	Dust
D2	True	True	True	0.14	Dust
D3	True	True	True	0.77	Dust
D4	True	True	True	0.39	Dust
D5	True	True	True	0.59	Dust
D6	False	False	True	0.13	Dust
D7	True	False	True	0.17	Dust

Note: The weather condition of each sample was defined by a combination of the above four factors.

[1] PM_{10} mass concentration: 'True' was defined as PM_{10} mass concentration larger than 200 μg m^{-3} for more than 2 hours.

[2] The volume concentration of the coarse mode particles (> 1 μm): 'True' was defined for mean concentration higher than 75 μm^3 cm^{-3}. The threshold was developed based on the measurements of 2004-2006 in Beijing. Asian dust loading has declined in recent years. Thus, this threshold is not mandatory.

[3] Phenomenological dust storm observations: China Meteorological Administration (CMA) provides predictions and observations on dust storm events that occurred in China. The dust events in Beijing identified in this study have been reported as the largescale dust storm events.

[4] Aluminium (Al) is usually selected to be an indicator of mineral dust because it is one of the most abundant constant elements in deserts. Thus, the concentration of Al is considered as an important factor to define dust events.

[5] Sample M4 was collected from the end of a continuous dust storm (M1, M2, and M3), i.e., during the removal process after a dust storm. High wind speeds can blow up large particles from the roads and other surfaces in the city. In addition, the air mass of M4 passed through the Bohai Sea before arriving in Beijing (Fig. S1), possibly bringing large marine particles. Although the average concentration of PM_{10} for sample M4 was higher than those of samples M5 and D6, the concentration of Al in sample M4 was much lower compared to sample M5 and D6. Therefore, we classify sample M4 as a non-dust event, since it's not dominated by mineral dust.

Table S2. The INP concentrations for 8 particle sizes at different temperatures. Three criteria (average concentration (Average), standard deviation (STD), and valid sample number (Sample Num)) based on 13 dust dominated samples are presented for each particle size. Large size particles start and complete freezing at warmer temperatures than small particles. At a given temperature, not all 13 samples may begin to freeze, while some samples may be completely frozen. Therefore, the valid sample number for the 8 particle sizes presented here at various temperatures is less than or equal to 13.

Particle size (μm)	Type	Temperature (°C) & INP concentrations (L^{-1})						
		-8	-10	-13	-15	-18	-20	-23
10.0	Average	0.055	0.150	0.481	0.786	2.244	3.904	7.577
	STD	0.066	0.198	0.627	0.890	1.673	2.297	4.527
	Sample Num	9	11	11	11	11	8	3
5.6	Average	0.117	0.247	0.615	1.030	2.395	3.913	4.542
	STD	0.212	0.437	1.004	1.553	1.987	2.943	3.621
	Sample Num	9	13	13	13	12	9	3
3.2	Average	0.064	0.184	0.552	0.993	2.830	4.228	8.722
	STD	0.117	0.211	0.537	1.031	2.300	2.916	/
	Sample Num	11	12	13	13	13	9	1
1.8	Average	0.042	0.119	0.329	0.618	2.059	3.289	4.121
	STD	0.064	0.147	0.340	0.540	1.714	2.518	3.373
	Sample Num	9	12	12	12	13	10	5
1.0	Average	0.028	0.065	0.156	0.289	1.005	2.610	4.017
	STD	0.025	0.053	0.145	0.272	0.867	2.206	3.388
	Sample Num	6	10	12	12	13	12	5
0.56	Average	0.012	0.025	0.048	0.096	0.429	1.574	3.686
	STD	0.004	0.016	0.036	0.076	0.297	1.092	3.768
	Sample Num	2	10	13	13	13	12	5
0.32	Average	0.010	0.021	0.040	0.059	0.275	1.143	1.481
	STD	0.006	0.018	0.045	0.066	0.359	1.821	0.920
	Sample Num	2	4	10	11	13	12	5
0.18	Average	0.010	0.009	0.016	0.022	0.081	0.226	0.286
	STD	0.006	0.005	0.014	0.028	0.090	0.280	0.125
	Sample Num	2	3	7	9	11	10	4

Table S3. The average percentage of heat-resistant and heat-sensitive INPs of the overall INP populations ($D_{50} \geq$ 1.0 μm) at three different temperatures. The indicated uncertainties correspond to the standard deviation of 12 samples at each temperature.

Type	Temperature (℃) & Average concentration proportion		
	-10 ℃	-15 ℃	-20 ℃
Heat-sensitive INPs	81 ± 12%	70 ± 15%	38 ± 21%
Heat- resistant INPs	19 ± 12%	30 ± 15%	62 ± 21%

80

Table S4. The average percentage of heat-resistant and heat-sensitive INPs of the size-resolved INPs ($D_{50} = 10.0, 5.6,$ 85 $3.2, 1.8\ and$ 1.0 μm) at different temperatures. The valid sample number (Sample Num) presented in the table is less than or equal to 12 because the results are based on 12 samples.

Temperature (℃)	Type	Particle size (μm) & Concentration proportion				
		10.0	5.6	3.2	1.8	1.0
-10	Heat-sensitive INPs	80%	78%	82%	89%	84%
	Heat- resistant INPs	20%	22%	18%	11%	16%
	Sample Num	10	12	11	11	9
-15	Heat-sensitive INPs	75%	64%	71%	75%	70%
	Heat- resistant INPs	25%	36%	29%	25%	30%
	Sample Num	10	12	12	11	11
-20	Heat-sensitive INPs	33%	27%	34%	35%	66%
	Heat- resistant INPs	67%	73%	66%	65%	34%
	Sample Num	10	12	12	12	12

90

Table S5. The average percentage of heat-resistant and heat-sensitive INPs of the northwest and north samples ($D_{50} \geq$ 1.0 μm) at two temperatures. The indicated uncertainties correspond to the standard deviation of samples in the same pathways.

Temperature (℃)	Sample type & Average concentration proportion			
	NW-HR[1]	NW-HS[2]	N-HR[3]	N-HS[4]
-10 ℃	12 ± 2%	88 ± 2%	31 ± 19%	69 ± 19%
-15 ℃	21 ± 3%	79 ± 3%	46 ± 20%	54 ± 20%

Note:

[1] NW-HR: Heat-resistant INPs of the northwest samples ($D_{50} \geq$ 1.0 μm, sample M6, M7, M8 and D7, the same below);

[2] NW-HS: Heat-sensitive INPs of the northwest samples;

[3] N-HR: Heat-resistant INPs of the north samples ($D_{50} \geq$ 1.0 μm, sample M3 and D6, the same below);

[4] N-HS: Heat-sensitive INPs of the north samples;

2. Supplementary Figures

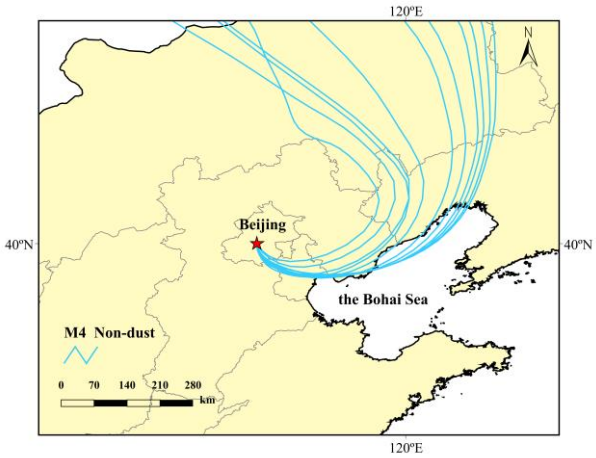

Figure S1. Back trajectory of the air mass for sample M4 (solid blue lines), which went through the Bohai Sea before arriving in Beijing.

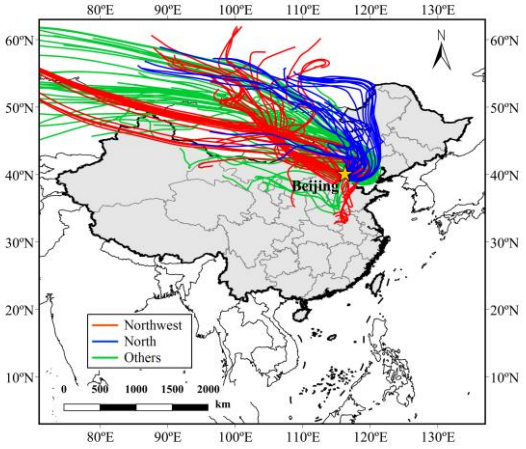

Figure S2. Air mass trajectories for different samples originated from the northwest (M6, M7, M8 and D7; solid red lines), north (M3, M5 and D6; solid blue lines) and other (M1, M2, D2, D3, D4 and D5; solid green lines) transport pathways.

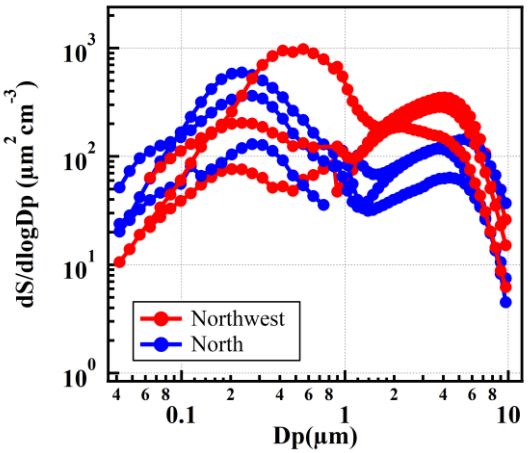

Figure S3. Surface area distributions of the northwest (M6, M7, M8 and D7) and north (M3, M5 and D6) transport pathways averaged over the respective sampling periods. D_p is the aerodynamic diameter of the particles. The surface area spectrum of the sample D7 is partially missing, and is not shown here.

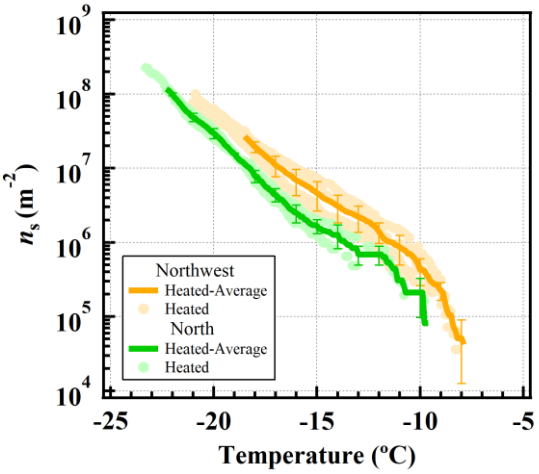

Figure S4. Comparison of nucleation activity of northwest and north samples after heat treatment. Northwest and north samples are named "Heated", and marked as solid light yellow/green circles, respectively. The average $n_s(T)$ of the samples in the same pathway are illustrated as solid lines with corresponding colors.

3. Supplementary Methods

Particle washing removal efficiency

We did an experiment of particle washing removal efficiency to ensure that particles were washed off the filters, as depicted in Fig. S5. The tested filter was collected from a dust event in 2018, and all the extraction processes were the same as those described in the manuscript except for the extraction time. This Nuclepore filter was completely submerged in 20 mL double-distilled water (resistivity of 18.2 MΩ·cm at 25 ℃) and was extracted by an ultrasonic shaker for 15 minutes to get the sample called "15 min - 1st" in Fig. S5. Then the filter was removed from the washed suspension and was immersed in a fresh 20 mL double-distilled water for a second extraction cycle to obtain the sample called "15 min - 2nd". The sample "15 min - 3rd" was produced similarly in a third extraction cycle.

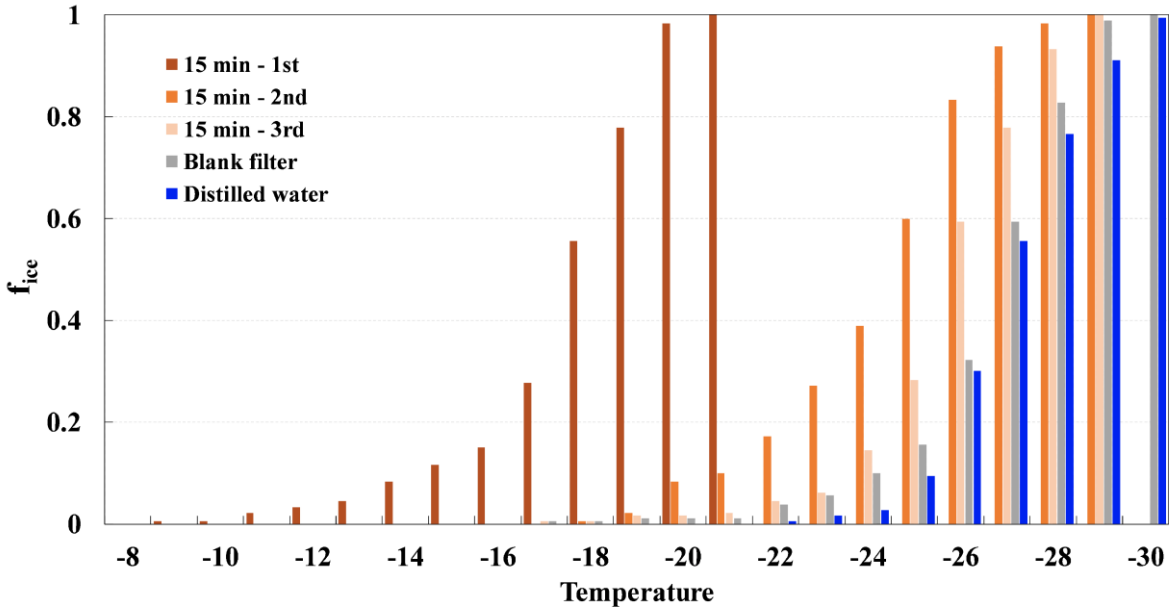

Figure S5. Particle washing removal efficiency experiments. The brown, orange and light orange bars represent the frozen fraction (f_{ice}) of the solution at different temperatures after the first, second, and third ultrasonic treatment, respectively. As comparisons, the grey and blue bars are the droplet freezing experiments for blank filter and distilled water, respectively.

The freezing of the three samples indicated that most of the particles were extracted efficiently in the first cycle, which had higher frozen fractions at higher temperatures than rest of the samples. Indeed, some of the particles remained over the filter, but a longer extraction periods would not impact the freezing results, since there was only minor overlap between their freezing temperatures. Therefore, 15-minute ultrasound treatments for twice (i.e., 30 minutes) can wash all ice active materials off the filters.

Determination of surface ice active site density ($n_s(T)$)

The surface ice active site density, $n_s(T)$,was derived from our measured data, as described in our manuscript. As a key parameter, the particle diameter (i.e., particle surface area) is a main uncertainty source for the calculation of $n_s(T)$, and the particle diameter should be specified when comparing the $n_s(T)$ values among different studies.

Two main diameters, geometric and BET-inferred diameters (derived from BET surface, a gas adsorption technique, Brunauer et al., 1938), were adopted in calculating $n_s(T)$, although some studies did not mention which particle sizes they used. It is clear that the BET-inferred surface area is typically larger than simplified spherical estimation, resulting in a lower $n_s(T)$ value if employed (Hiranuma et al., 2015).

We evaluated the bias of the results calculated using aerodynamic and geometric diameter. The geometric diameter can be converted from its aerodynamic diameter as:

$$D_{\mathrm{ae}} = D_g \sqrt{\frac{\rho_p C_{\mathrm{g}}}{\rho_0 C_{\mathrm{ae}} \chi}}$$

where D_{ae} is aerodynamic diameter, D_g is geometric diameter (i.e., the volume equivalent diameter), ρ_0 is unit density (1 g cm^{-3}), ρ_p is the particle density, χ is the dynamic shape factor, C_g and C_{ae} are the Cunningham slip correction factors associated with the geometric and aerodynamic diameters, respectively.

Table S6. The deviation of calculations between the geometric and aerodynamic diameters

ρ_p (g cm^{-3})	χ	D_{ae}	D_g	$n_s(T)$[a]	
2.6	1.1	D_{ae}	$D_g = 0.65\ D_{\mathrm{ae}}$	$n_{s,g} = 2.36\ n_{s,ae}$	$n_{s,ae} = 0.42\ n_{s,g}$
2.0	1.1	D_{ae}	$D_g = 0.74\ D_{\mathrm{ae}}$	$n_{s,g} = 1.82\ n_{s,ae}$	$n_{s,ae} = 0.55\ n_{s,g}$
1.8	1.1	D_{ae}	$D_g = 0.78\ D_{\mathrm{ae}}$	$n_{s,g} = 1.64\ n_{s,ae}$	$n_{s,ae} = 0.61\ n_{s,g}$
1.5	1.1	D_{ae}	$D_g = 0.86\ D_{\mathrm{ae}}$	$n_{s,g} = 1.36\ n_{s,ae}$	$n_{s,ae} = 0.74\ n_{s,g}$
2.6	1.4	D_{ae}	$D_g = 0.73\ D_{\mathrm{ae}}$	$n_{s,g} = 1.86\ n_{s,ae}$	$n_{s,ae} = 0.54\ n_{s,g}$
2.0	1.4	D_{ae}	$D_g = 0.84\ D_{\mathrm{ae}}$	$n_{s,g} = 1.43\ n_{s,ae}$	$n_{s,ae} = 0.70\ n_{s,g}$
1.8	1.4	D_{ae}	$D_g = 0.88\ D_{\mathrm{ae}}$	$n_{s,g} = 1.29\ n_{s,ae}$	$n_{s,ae} = 0.78\ n_{s,g}$
1.5	1.4	D_{ae}	$D_g = 0.97\ D_{\mathrm{ae}}$	$n_{s,g} = 1.07\ n_{s,ae}$	$n_{s,ae} = 0.93\ n_{s,g}$

[a] $n_{s,g}$ and $n_{s,ae}$ are the surface ice active site densities associated with the geometric and aerodynamic diameters, respectively.

Table S6 shows the results of calculations using different particle densities (ρ_p = 1.5 - 2.6 g cm^{-3}) and dynamic shape factors (χ = 1.1 - 1.4, Niemand et al., 2012) when the slip correction factor is not considered. At a given particle density and

dynamic shape factor, D_g is 0.65 to 0.97 times D_{ae}, and $n_{s,g}$ is 1.07 to 2.36 times $n_{s,ae}$. Therefore, our $n_s(T)$ derived from the aerodynamic diameter is 0.42 to 0.93 times the value of $n_s(T)$ determined by the converted geometric diameter.

We choose to use the aerodynamic diameter rather than the converted geometric diameter to derive the $n_s(T)$ values for three reasons. First, the conversion between aerodynamic and geometric diameters requires knowledge of particle density and shape factor. However, the above two parameters are associated with the chemical composition, diameter and morphology of particles, and cannot be measured directly. There is large uncertainty when using estimated fixed values. In fact, the Cunningham slip correction factor, which is often neglected in calculations, is also an important factor for particles smaller than 1 μm. Second, the determination of geometric diameter is influenced by the wavelength of the measuring instrument. Third, the airborne particles collected in our measurement were mixed particles rather than pure mineral dust, and the size distribution was mainly detected by APS. We think the uncertainty would be reduced to the greatest extent when using the aerodynamic particle size in calculation.

In a word, we use the aerodynamic diameter in calculating $n_s(T)$, and note that the uncertainty should be borne in mind when comparing our data with other studies.

References

Brunauer, S., Emmett, P. H., and Teller, E.: Adsorption of Gases in Multimolecular Layers, Journal of the American Chemical Society, 60, 309-319, 10.1021/ja01269a023, 1938.

Hiranuma, N., Augustin-Bauditz, S., Bingemer, H., Budke, C., Curtius, J., Danielczok, A., Diehl, K., Dreischmeier, K., Ebert, M., Frank, F., Hoffmann, N., Kandler, K., Kiselev, A., Koop, T., Leisner, T., Mohler, O., Nillius, B., Peckhaus, A., Rose, D., Weinbruch, S., Wex, H., Boose, Y., DeMott, P. J., Hader, J. D., Hill, T. C. J., Kanji, Z. A., Kulkarni, G., Levin, E. J. T., McCluskey, C. S., Murakami, M., Murray, B. J., Niedermeier, D., Petters, M. D., O'Sullivan, D., Saito, A., Schill, G. P., Tajiri, T., Tolbert, M. A., Welti, A., Whale, T. F., Wright, T. P., and Yamashita, K.: A comprehensive laboratory study on the immersion freezing behavior of illite NX particles: a comparison of 17 ice nucleation measurement techniques, Atmospheric Chemistry and Physics, 15, 2489-2518, 10.5194/acp-15-2489-2015, 2015.

Niemand, M., Möhler, O., Vogel, B., Vogel, H., Hoose, C., Connolly, P., Klein, H., Bingemer, H., DeMott, P., Skrotzki, J., and Leisner, T.: A Particle-Surface-Area-Based Parameterization of Immersion Freezing on Desert Dust Particles, Journal of the Atmospheric Sciences, 69, 3077-30/10.1175 ,92jas-d-11-0249.1, 2012.